

1 **Feasibility analysis of using inverse modeling for estimating field-scale evapotranspiration in**
2 **maize and soybean fields from soil water content monitoring networks**

3
4 Foad Foolad¹, Trenton E. Franz², Tiejun Wang^{2,3}, Justin Gibson², Ayse Kilic^{1,2}, Richard G. Allen⁴,
5 Andrew Suyker²

6
7 ¹Civil Engineering Department, University of Nebraska-Lincoln, USA

8 ²School of Natural Resources, University of Nebraska-Lincoln, USA

9 ³Institute of Surface-Earth System Science, Tianjin University, P.R. China

10 ⁴Kimberly Research and Extension Center, University of Idaho, USA

11
12 **Keywords:** Evapotranspiration; Soil Water Content; Inverse Modeling; Soil Hydraulic Parameters;
13 Cosmic-Ray Neutron Probe

14 Corresponding author T.E. Franz (tfranz2@unl.edu)

15

16

17

18

19 **Abstract**

20 In this study the feasibility of using inverse vadose zone modeling for estimating field scale actual
21 evapotranspiration (ET_a) was explored at a long-term agricultural monitoring site in eastern
22 Nebraska. Data from both point scale soil water content (SWC) sensors and the area-average
23 technique of Cosmic-Ray Neutron Probes were evaluated against independent ET_a estimates from
24 a co-located Eddy-Covariance tower. While this methodology has been successfully used for
25 estimates of groundwater recharge, it was essential to assess the performance of other components
26 of the water balance such as ET_a . In light of recent evaluations of Land Surface Models (LSM)
27 independent estimates of hydrologic state variables and fluxes are critically needed benchmarks.
28 The results here indicate reasonable estimates of daily and annual ET_a from the point sensors, but
29 with highly varied soil hydraulic function parameterizations due to local soil texture variability.
30 The results of multiple soil hydraulic parameterizations leading to equally good ET_a estimates is
31 consistent with the hydrological principle of equifinality. While this study focused on one
32 particular site, the framework can be easily applied to other SWC monitoring networks across the
33 globe. The value added products of groundwater recharge and ET_a flux from the SWC monitoring
34 networks will provide additional and more robust benchmarks for the validation of LSM that
35 continues to improve their forecast skill. In addition, the value added products of groundwater
36 recharge and ET_a often have more direct impacts on societal decision making than SWC alone.
37 Water flux impacts human decision making from policies on the long-term management of
38 groundwater resources (recharge), to yield forecasts (ET_a), and to optimal irrigation scheduling
39 (ET_a). Illustrating the societal benefits of SWC monitoring is critical to insure the continued
40 operation and expansion of these public datasets.

41

42 **1. Introduction**

43 Evapotranspiration (ET) is an important component in terrestrial water and surface energy
44 balance. In the United States, ET comprises about 75% of annual precipitation, while in arid and
45 semiarid regions ET comprises more than 90% of annual precipitation (Zhang et al., 2001; Glenn
46 et al., 2007; Wang et al., 2009a). As such, an accurate estimation of ET is critical in order to
47 predict changes in hydrological cycles and improve water resource management (Suyker et al.,
48 2008; Anayah and Kaluarachchi, 2014). Given the importance of ET , an array of measurement
49 techniques at different temporal and spatial scales have been developed (c.f., Maidment, 1992;
50 Zhang et al., 2014), including lysimeter, Bowen ratio, Eddy-Covariance (EC), and satellite-based
51 surface energy balance approaches. However, simple, low-cost, and accurate field-scale
52 measurements of actual ET (ET_a) still remain a challenge due to the uncertainties of available
53 estimation techniques (Wolf et al., 2008; Li et al., 2009; Senay et al., 2011; Stoy, 2012). For
54 instance, field techniques, such as EC and Bowen ratio, can provide relatively accurate estimation
55 of local ET_a , but are often cost prohibitive for wide-spread use beyond research applications
56 (Baldocchi et al., 2001; Irmak, 2010). By comparison, satellite-based remote sensing techniques
57 are far less costly for widespread spatial coverage (Allen et al., 2007), but are limited by their
58 accuracy, temporal sampling frequency (e.g., Landsat 8 has a 16-day overpass), and technical
59 issues that further limit temporal sampling periods (e.g., cloud coverage during overpass) (Chemin
60 and Alexandridis, 2001; Xie et al., 2008; Li et al., 2009; Kjaersgaard et al., 2012).

61 As a complement to the above mentioned techniques, recent studies have used process-
62 based vadose zone models (VZMs) for estimating field-scale ET_a with reasonable success,
63 particularly in arid and semi-arid areas (Twarakavi et al., 2008; Izadifar and Elshorbagy, 2010;
64 Galleguillos et al., 2011; Wang et al., 2016). Although VZMs are time and cost effective for

65 estimating field-scale ET_a , they generally require complex model parameterizations and inputs,
66 some of which are not readily available (e.g., soil hydraulic parameters and plant physiological
67 parameters; c.f. Wang et al., 2016). In order to address the issue of missing soil hydraulic
68 parameters, a common approach is to use pedotransfer functions to convert readily available soil
69 information (e.g., texture, bulk density, etc.) to soil hydraulic parameters (Wösten et al., 2001);
70 however, significant uncertainties are usually associated with this method for estimating local
71 scale water fluxes (Wang et al., 2015). In fact, Nearing et al. (2016) identified soil hydraulic
72 property estimation as the largest source of information lost when evaluating different land surface
73 modeling schemes versus a soil moisture benchmark. Poor and uncertain parameterization of soil
74 hydraulic properties is a clear weakness of land surface models (LSMs) predictive skill in sensible
75 and latent heat fluxes (Best et al., 2015). This problem will continue to compound with the
76 continuing spatial refinement of hyper-resolution LSM grid cells to less than 1 km (Wood et al.,
77 2011).

78 In order to address the challenge of field scale estimation of soil hydraulic properties, here
79 we utilize inverse modeling for estimating soil hydraulic parameters based on field measurements
80 of soil water content (SWC) (c.f. Hopmans and Šimunek, 1999; Ritter et al., 2003). While VZM-
81 based inverse approaches have already been examined for estimating groundwater recharge (e.g.,
82 Jiménez-Martínez et al., 2009; Andreasen et al., 2013; Min et al., 2015; Ries et al., 2015;
83 Turkeltaub et al., 2015; Wang et al., 2016), its application for ET_a estimation has not been
84 adequately tested. Moreover, we note that simultaneous estimation of SWC states and surface
85 energy fluxes within LSMs is complicated by boundary conditions, model parameterization, and
86 model structure (Nearing et al., 2016). With the incorporation of regional soil datasets in LSMs
87 like Polaris (Chaney et al., 2016), effective strategies for estimating ground truth soil hydraulic

88 properties from existing *SWC* monitoring networks (e.g., SCAN, CRN, COSMOS, State/National
89 Mesonets, c.f. Xia et al. (2015)) will become critical for continuing to improve the predictive skill
90 of LSMs.

91 The aim of this study is to examine the feasibility of using inverse VZM for estimating
92 field scale ET_a based on long-term local meteorological and *SWC* observations for an Ameriflux
93 (Baldocchi et al., 2001) EC site in eastern Nebraska, USA. We note that while this study focused
94 on one particular study site in eastern Nebraska, the methodology can be easily adapted to a
95 variety of *SWC* monitoring networks across the globe (Xia et al., 2015), thus providing an
96 extensive set of benchmark data for use in LSMs. The remainder of the paper is organized as
97 follows. In the methods section we will describe the widely used VZM, Hydrus-1D (Šimunek et al.,
98 2013), used to obtain soil hydraulic parameters. We will assess the feasibility of using both
99 profiles of in-situ *SWC* probes as well as the area-average *SWC* technique from Cosmic-Ray
100 Neutron Probes (CRNP). In the results section we will compare simulated ET_a resulted from
101 calibrated VZM with independent ET_a estimates provided by EC observations. Finally, a
102 sensitivity analysis of key soil and plant parameters will be presented.

103

104 **2. Materials and Methodology**

105 **2.1 Study Site**

106 The study site is located in eastern Nebraska, USA at the University of Nebraska
107 Agricultural and Development Center near Mead. The field site (US-Ne3, Figure 1a, 41.1797° N,
108 96.4397° W) is part of the Ameriflux Network (Baldocchi et al., 2001) and has been operating
109 continually since 2001. The regional climate is of a continental semiarid type with a mean annual

110 precipitation of 784 mm/year (according to the Ameriflux US-Ne3 website). According to the Web
111 Soil Survey Data (Soil Survey Staff, 2016, <http://websoilsurvey.nrcs.usda.gov/>), the soils at the site
112 are comprised mostly of silt loam and silty clay loam (Figure 1b and Table 1). Soybean and maize
113 are rotationally grown at the site under rainfed conditions, with the growing season beginning in
114 early May and ending in October (Kalfas et al., 2011). Since 2001, crop management practices (i.e.,
115 planting density, cultivars, irrigation, and herbicide and pesticide applications) have been applied
116 in accordance with standard best management practices prescribed for production-scale maize
117 systems (Suyker et al., 2008). More detailed information about site conditions can be found in
118 Suyker et al. (2004) and Verma et al. (2005).

119 An EC tower was constructed at the center of the field (Figure 1 and Figure 2a), which
120 continuously measures water, energy, and CO₂ fluxes (e.g., Baldocchi et al., 1988). At this field,
121 sensors are mounted at 3.0 m above the ground when the canopy is shorter than 1.0 m. At canopy
122 heights greater than 1.0 m, the sensors are then moved to a height of 6.2 m until harvest in order to
123 have sufficient upwind fetch (in all directions) representative of the cropping system being studied
124 (Suyker et al., 2004). In this study, hourly latent heat flux measurements were integrated to daily
125 values and then used for calculating daily EC ET_a integrated over the field scale. Detailed
126 information on the EC measurements and calculation procedures for ET_a are given in Suyker and
127 Verma (2009). Hourly air temperature, relative humidity, horizontal wind speed, net radiation, and
128 precipitation were also measured at the site. Destructive measurements of leaf area index (LAI)
129 were made every 10 to 14 days during the growing season at the study site (Suyker et al., 2005).
130 We note that the LAI data were linearly interpolated to provide daily estimates. Theta probes (TP)
131 (Delta-T Devices, Cambridge, UK) were installed at 4 locations in the study field with
132 measurement depths of 10, 25, 50, and 100 cm at each location to monitor hourly SWC in the root

133 zone (Suyker et al., 2008). Here, we denote these four locations as TP 1 (41.1775° N, 96.4442° W),
134 TP 2 (41.1775° N, 96.4428° W), TP 3 (41.1775° N, 96.4402° W), and TP 4 (41.1821° N, 96.4419°
135 W) (Figure 1b). Daily precipitation (P) and reference evapotranspiration (ET_r) computed for the
136 tall (alfalfa) reference crop using the ASCE standardized Penman-Monteith equation (ASCE-
137 EWRI 2005) are shown in Figure 3 for the study period (2007–2012) at the study site.

138 In addition, a CRNP (model CRS 2000/B, HydroInnova LLC, Albuquerque, NM, USA,
139 41.1798 N°, 96.4412° W) was installed near the EC tower (Figure 1b and 2b) on 20 April 2011.
140 The CRNP measures hourly moderated neutron counts (Zreda et al., 2008, 2012), which are
141 converted into SWC following standard correction procedures and calibration methods (c.f., Zreda
142 et al., 2012). In addition, the changes in above-ground biomass were removed from the CRNP
143 estimates of SWC following Franz et al. (2015). The CRNP measurement depth (Franz et al., 2012)
144 at the site varies between 15-40 cm, depending on SWC . Note for simplicity in this analysis we
145 assume the CRNP has an effective depth of 20 cm (mean depth of 10 cm) for all observational
146 periods. The areal footprint of the CRNP is $\sim 250 \pm 50$ m radius circle (see Desilets and Zreda
147 2013 and Köhli et al., 2015 for details). Here we assume for simplicity the EC and CRNP
148 footprints are both representative of the areal-average field conditions.

149

150 **2.2. Model setup**

151 **2.2.1 Vadose Zone Model**

152 The Hydrus-1D model (Šimunek et al., 2013), which is based on the Richards equation,
153 was used to calculate ET_a . The setup of the Hydrus-1D model is explained in detail by Jiménez-
154 Martínez et al. (2009), Min et al. (2015), and Wang et al. (2016), and only a brief description of

155 the model setup is provided here. Given the measurement depths of the Theta Probes, the
156 simulated soil profile length was chosen to be 175 cm with 176 nodes at 1 cm intervals. An
157 atmospheric boundary condition with surface runoff was selected as the upper boundary. This
158 allowed the occurrence of surface runoff when precipitation rates were higher than soil infiltration
159 capacity or if the soil became saturated. According to a nearby USGS monitoring well (Saunders
160 County, NE, USGS 411005096281502, ~2.7 km away), the depth to water tables was greater than
161 12 m during the study period. Therefore, free drainage was used as the lower boundary condition.

162 Based on ASCE Penman-Monteith equation, ET_r values can be computed for either grass
163 or alfalfa and then using crop-specific coefficients daily potential evapotranspiration (ET_p) can be
164 calculated. Here daily ET_r values were calculated for the tall (0.5 m) ASCE reference (ASCE-
165 EWRI, 2005), and daily potential evapotranspiration (ET_p) was calculated according to FAO 56
166 (Allen et al., 1998):

$$167 \quad ET_p(t) = K_c(t) \times ET_r(t) \quad (1)$$

168 where K_c is a crop-specific coefficient at time t . The estimates of growth stage lengths and K_c
169 values for maize and soybean suggested by Allen et al. (1998) and Min et al. (2015) were adopted
170 in this study. In order to partition daily ET_p into potential transpiration (T_p) and potential
171 evaporation (E_p) as model inputs, Beer's law (Šimunek et al., 2013) was used as follows:

$$172 \quad E_p(t) = ET_p(t) \times e^{-k \times LAI(t)} \quad (2)$$

$$173 \quad T_p(t) = ET_p(t) - E_p(t) \quad (3)$$

174 where k [-] is an extinction coefficient with a value set to 0.5 (Wang et al., 2009b) and LAI [L^2/L^2]
 175 is leaf area index described in the previous section. The root water uptake, $S(h)$, was simulated
 176 according to the model of Feddes et al. (1978):

$$177 \quad S(h) = \alpha(h) \times S_p \quad (4)$$

178 where $\alpha(h)$ [-] is the root-water uptake water stress response function and varies between 0 and 1
 179 depending on soil matric potentials, and S_p is the potential water uptake rate and assumed to be
 180 equal to T_p . The summation of actual soil evaporation and actual transpiration is ET_a .

181 Since the study site has annual cultivation rotations between soybean and maize, the root
 182 growth model from the Hybrid-Maize Model (Yang et al., 2004) was used to model the root
 183 growth during the growing season:

$$184 \quad \begin{cases} \text{if } D < MRD, D = \frac{AGDD}{GDD_{Silking}} MRD \\ \text{or } D = MRD \end{cases} \quad (5)$$

185 where D (cm) is plant root depth for each growing season day, MRD is the maximum root depth
 186 (assumed equal to 150 cm for maize and 120 cm for soybean in this study following Yang et al.,
 187 2004), $AGDD$ is the accumulated growing degree days, and $GDD_{Silking}$ is the accumulated GDD at
 188 the silking point (e.g., accumulated plant GDD approximately 60-70 days after crop emergence).
 189 GDD for each growing season day was calculated as:

$$190 \quad GDD = \frac{T_{max} - T_{min}}{2} - T_{base} \quad (6)$$

191 where T_{max} and T_{min} are the maximum and minimum daily temperature ($^{\circ}C$), respectively, and T_{base}
 192 is the base temperature set to be $10^{\circ} C$ following McMaster and Wilhelm (1997) and Yang et al.

193 (1997). Finally, the Hoffman and van Genuchten (1983) model was used to calculate root
194 distribution. Further details about the model can be found in Šimunek et al. (2013).

195

196 2.2.2 Inverse modeling to estimate soil hydraulic parameters

197 Inverse modeling was used to estimate soil hydraulic parameters for the van Genuchten-
198 Mualem model (Mualem, 1976; van Genuchten, 1980):

$$199 \theta(h) = \begin{cases} \theta_r + \frac{\theta_s - \theta_r}{(1 + |\alpha h|^n)^m}, & h < 0 \\ \theta_s, & h \geq 0 \end{cases} \quad (7)$$

$$200 K(S_e) = K_s \times S_e^l \times [1 - (1 - S_e^{1/m})^m]^2 \quad (8)$$

201 where θ [L^3/L^3] is volumetric *SWC*; θ_r [L^3/L^3] and θ_s [L^3/L^3] are residual and saturated water
202 content, respectively; h [L] is pressure head; K [L/T] and K_s [L/T] are unsaturated and saturated
203 hydraulic conductivity, respectively; and $S_e (= (\theta - \theta_r) / (\theta_s - \theta_r))$ [-] is saturation degree. With respect
204 to the fitting factors, α [1/L] is inversely related to air entry pressure, n [-] measures the pore size
205 distribution of a soil with $m=1-1/n$, and l [-] is a parameter accounting for pore space tortuosity
206 and connectivity.

207 Daily *SWC* data from the four TP locations and CRNP location were used for the inverse
208 modeling. Based on the measurement depths of the TPs, the simulated soil columns were divided
209 into four layers for TP locations (i.e., 0-15 cm, 15-35 cm, 35-75 cm, and 75-175 cm), which led to
210 a total of 24 hydraulic parameters (θ_r , θ_s , α , n , K_s , and l) to be optimized based on observed *SWC*
211 values. In order to efficiently optimize the parameters, we used the method outlined in Turkeltaub
212 et al. (2015). Since Hydrus-1D is limited to optimizing a maximum of 15 parameters at once and

213 that the *SWC* of the lower layers changes more slowly and over a smaller range than the upper
214 layers, the van Genuchten parameters of the upper two layers were first optimized, while the
215 parameters of the lower two layers were fixed. Then, the optimized van Genuchten parameters of
216 the upper two layers were kept constant, while the parameters of the lower two layers were
217 optimized. The process was continued until there were no further improvements in the optimized
218 hydraulic parameters or until the changes in the lowest sum of squares were less than 0.1%. Given
219 the sensitivity of the optimization results to the initial guesses of soil hydraulic parameters in the
220 Hydrus model, soil hydraulic parameters from six soil textures were used as initial inputs for the
221 optimizations at each location (Carsel and Parish, 1988), including sandy clay loam, silty clay
222 loam, loam, silt loam, silt, and clay loam. Based on the length of available *SWC* data from the TP
223 measurements, the periods of 2007, 2008-2010, and 2011-2012 were used as the spin-up,
224 calibration, and validation periods, respectively. Moreover, to minimize the impacts of freezing
225 conditions on the quality of *SWC* measurements, data from January to March of each calendar year
226 were removed (based on available soil temperature data) from the optimizations.

227 In addition to the TP profile observations, we used the CRNP area-average *SWC* in the
228 inverse procedure to develop an independent set of soil parameters. The CRNP was assumed to
229 provide *SWC* data with an average effective measurement depth of 20 cm at this study site. The
230 observation point was therefore set at 10 cm. As a first guess and in the absence of other
231 information, soil properties were assumed to be homogeneous throughout the simulated soil
232 column with a length of 175 cm. Because the CRNP was installed in 2011 at the study site, the
233 periods of 2011, 2012-2013, and 2014 were used as spin-up, calibration, and validation periods,
234 respectively, for the optimization procedure.

235 The lower and upper bounds of each van Genuchten parameter are provided in Table 2.
 236 With respect to the goodness-of-fit assessment, Root Mean Square Error (RMSE) between
 237 simulated and observed *SWC* was chosen as the objective function to minimize in order to estimate
 238 the soil hydraulic parameters. The built in optimization procedure in Hydrus-1D was used to
 239 perform parameter estimation. A sensitivity analysis of the six soil model parameters was
 240 performed. In addition, three additional performance criteria, including Coefficient of
 241 Determination (R^2), Mean Average Error (MAE), and the Nash-Sutcliffe Efficiency (NSE) were
 242 used to further evaluate and validate the selected model behavior:

$$243 \quad RMSE = \sqrt{\frac{1}{n} \sum_{i=1}^n (P_i - O_i)^2} \quad (9)$$

$$244 \quad R^2 = \left(\frac{n(\sum_{i=1}^n P_i O_i) - (\sum_{i=1}^n P_i)(\sum_{i=1}^n O_i)}{\sqrt{[n \sum_{i=1}^n P_i^2 - (\sum_{i=1}^n P_i)^2][n \sum_{i=1}^n O_i^2 - (\sum_{i=1}^n O_i)^2]}} \right)^2 \quad (10)$$

$$245 \quad MAE = \frac{1}{n} \sum_{i=1}^n |P_i - O_i| \quad (11)$$

$$246 \quad NSE = 1 - \frac{\sum_{i=1}^n (P_i - O_i)^2}{\sum_{i=1}^n (O_i - \bar{O}_i)^2} \quad (12)$$

247 where n is the total number of *SWC* data points, O_i , and P_i , are respectively the observed and
 248 simulated daily *SWC* on day i , and \bar{O}_i is the observed mean value. Based on the best scores (i.e.,
 249 lowest RMSE values), the best optimized set of soil hydraulic parameters at each location were
 250 selected. Using the selected parameters, the Hydrus model was then run in a forward mode in order
 251 to estimate ET_a between 2007 and 2012. Finally, we note that the years 2004-2006 were used as a
 252 model spin-up period for the forward model and evaluation of ET_a because of the longer climate
 253 record length.

254

255 3. Results and Discussions

256 3.1 Vadose Zone Inverse Modeling Results

257 The time series of the average *SWC* from the four TP locations along with one standard
258 deviation at each depth are plotted in Figure 4. Based on the large spatial standard deviation values
259 (Figure 4), despite the relatively small spatial scale (~65 ha) and uniform cropping at the study site,
260 *SWC* varies considerably across the site, particularly during the growing season. The comparison
261 between *SWC* data from the CRNP and spatial average of *SWC* data at the four TP locations in the
262 study field (i.e. average of 10 and 25 cm depths at TP locations) is presented in Figure 5. The daily
263 RMSE between the spatial average of the TPs and CRNP data is $0.037 \text{ cm}^3/\text{cm}^3$, which is
264 consistent with other studies that reported similar values in semiarid shrublands (Franz et al., 2012),
265 German Forests (Bogena et al., 2013, Baatz et al., 2014), montane forests in Utah (Lv et al., 2014),
266 sites across Australia (Hawdon et al., 2014), and a mixed land use agricultural site in Austria
267 (Franz et al. 2016). We note that we would expect lower RMSE ($\sim < 0.02 \text{ cm}^3/\text{cm}^3$) with additional
268 point sensors located at shallower depths and in more locations distributed across the study site.
269 Nevertheless, the consistent behavior between the spatial mean *SWC* of TPs and the CRNP allows
270 us to explore spatial variability of soil hydraulic properties within footprint using inverse modeling.
271 This will be described in the next sections. The study period (2007-2012, Figure 6) contained
272 significant inter-annual variability in precipitation. During the spin-up period in 2007, the annual
273 precipitation (942 mm) was higher than the mean annual precipitation (784 mm), 2008 was a wet
274 year (997 mm), 2009-2011 were near average years (715 mm), and 2012 was a record dry year
275 (427 mm) with widespread drought across the region. Therefore, both wet and dry years were
276 considered in the inverse modeling simulation period.

277 As an illustration, Figure 7 shows the daily observed and simulated *SWC* during the
278 calibration (2008–2010) and validation (2011–2012) periods at the TP 1 location (the simulation
279 results of the other three sites can be found in the supplemental Figures S1, S2, and S3). The
280 results of objective function criterion (RMSE) and the other three performance criteria (e.g., R^2 ,
281 MAE, and NSE) between simulated and observed *SWC* values at TPs locations are presented in
282 Table 3.

283 In this research we define RMSE values less than $0.03 \text{ cm}^3/\text{cm}^3$ between observed and
284 simulated *SWC* values as well-matched and RMSE between 0.03 and $0.06 \text{ cm}^3/\text{cm}^3$ as fairly well-
285 matched. We note the target error range of satellite *SWC* products (e.g. SMOS and SMAP) is less
286 than $0.04 \text{ cm}^3/\text{cm}^3$ (Entekhabi et al., 2010). Similar to previous studies (e.g., Jiménez-Martínez et
287 al., 2009; Andreasen et al., 2013; Min et al., 2015; Wang et al., 2016), the results of all the
288 performance criteria at TP locations show the capability of inverse modeling in estimation of soil
289 hydraulic parameters. The results of the calibration period (2008-2010) indicate that the simulated
290 and observed *SWC* values are in good agreement (i.e. well matched as defined above) throughout
291 the entire period at most locations and depths (Figure 7 and Table 3). In addition, the simulated
292 and observed *SWC* data are fairly well-matched at most locations and depths during the validation
293 period (2011-2012), with notable differences during the second half of 2012 during the extreme
294 drought conditions (Figure 7 and Table 3). Reasons for this disagreement in the observed and
295 simulated *SWC* data will be discussed in the following sections.

296 The results of inverse modeling using the CRNP data also indicate the feasibility of using
297 these data to estimate effective soil hydraulic parameters (Figure 8 and Table 4). Based on the
298 performance criteria (Table 4), the simulated data are fairly well-matched with the observed *SWC*
299 data during both the calibration and validation periods. Additional information from deeper soil

300 probes or more complex modeling approaches such as data assimilation techniques (Rosolem et al.,
301 2014, Renzullo et al., 2014) may be needed to fully utilize the CRNP data for the entire growing
302 season. However, this was beyond the scope of the current study and merits further investigation
303 given the global network of CRNP (Zreda et al., 2012) dating back to ~2011.

304 Table 5 summarizes the optimized van Genuchten parameters for the four different depths
305 of the four TP locations and the single layer for the CRNP location. The optimized parameters
306 were then used to estimate ET_a for the entire study period as an independent comparison to the EC
307 ET_a data. The results of the ET_a evaluation will be discussed in the next section. According to the
308 simulation results (Table 5), in most of the soil layers, the TP 4 location results in lower n , K_s , and
309 higher θ_r values than the other 3 locations (TPs 1-3), suggesting either underlying soil texture
310 variability in the field or texture dependent sensor sensitivity/calibration. As a validation for the
311 simulation results, the publicly available Web Soil Survey Data
312 (<http://websoilsurvey.nrcs.usda.gov/>) was used to explore whether the optimized van Genuchten
313 parameters from the inverse modeling (Figure 1b and Table 2) agreed qualitatively with the survey
314 data. Based on the Web Soil Survey Data, the soil at the TP 4 location contains higher clay
315 percentage than the other locations. Meanwhile, the optimized parameters reflect the spatial pattern
316 of soil texture in the field as shown by the Web Soil Survey Data (e.g., lower n and K_s values and
317 higher θ_r values at the TP 4 location with finer soil texture). Physically, finer-textured soils
318 generally have lower K_s and higher θ_r values (Carsel and Parrish, 1988). Moreover, the shape
319 factor n is indicative of pore size distributions of soils. In general, finer soils with smaller pore
320 sizes tend to have lower n values (Carsel and Parrish, 1988). The observed SWC at the TP 4
321 location is consistently higher than the average SWC of the other three locations (Figure S4 in
322 supplemental materials), which can be partly attributed to the higher θ_r values at the TP 4 location

323 (Wang and Franz, 2015). Overall, the obtained van Genuchten parameters from the inverse
324 modeling are in qualitatively good agreement with the available spatial distribution of soil texture
325 in the study field, indicating the capability of using inverse VZM to infer soil hydraulic properties.
326 Further work on validating the Web Soil Survey Data soil hydraulic property estimates is of
327 general interest to the LSM community.

328

329 **3.2 Comparison of modeled ET_a with observed ET_a**

330 Because a longer set of climatic data was available at the study site (as compared to *SWC*
331 data), we used 2004-2006 as a spin-up period. Using the best fit soil hydraulic parameters for the
332 four TP locations and the single CRNP location, the Hydrus-1D model was then run in a forward
333 mode to calculate ET_a over the entire study period (2007-2012). The simulated daily ET_a was then
334 compared with the independent EC ET_a measurements using RMSE (Eq. (9)) as the evaluation
335 criterion. In order to upscale TP ET_a estimation to the field/EC scale, we used the soil textural
336 boundaries and areas defined by the Web Soil Survey Data map to compute a weighted average
337 ET_a . In this research we consider RMSE values less than 1 mm/day between observed and
338 simulated ET_a values as well-matched and RMSE values between 1 and 1.2 as fairly well-matched
339 (Figure 9 and Table 6). The performance criterion results indicate that the simulated daily ET_a is in
340 a better agreement with EC ET_a measurements at the TP 1-3 locations than at the TP 4 and CRNP
341 locations (Table 6). However, based on the performance criteria from inverse modeling results and
342 on the Web Soil Survey Data, we conclude that spatial heterogeneity of soil texture in the study
343 field results in significant spatial variation in ET_a rates across the field (e.g., less ET_a occurs at the
344 TP 4 location than from the other parts of the field). Here smaller ET_a rates at the TP 4 location are

345 likely due to finer soil texture at this location, which makes it more difficult for the plant/roots to
346 overcome potentials to extract water from the soil, thus leading to a lower ET_a rate and greater
347 plant stress. In addition, higher surface runoff can be expected at the TP 4 location due to finer-
348 textured soils (as we observed during our field campaigns). According to the simulation results the
349 average surface runoff at the TP 4 location was about 44.8 mm/year from 2007 to 2012, while the
350 average surface runoff at the other three locations (TPs 1-3) was around 10.6 mm/year, which
351 partially accounts for the lower ET_a rates. We note that future work using historic yield maps may
352 also be used to further elucidate the soil hydraulic property differences given the direct correlation
353 between transpiration and yield.

354 Given that CRNPs have a limited observational depth and that only one single soil layer
355 was optimized in the inverse model for the CRNP, one could expect the simulated daily ET_a from
356 the CRNP to have larger uncertainty. Here we found an RMSE of 1.14 mm/day using the CRNP
357 versus 0.91 mm/day for the upscaled TP locations. However, when the optimized soil parameters
358 obtained from the CRNP data were used to estimate ET_a , the model did simulate daily ET_a fairly
359 well during both non-growing and growing seasons in comparison to the EC ET_a measurements.

360 On the annual scale, ET_a measured by the EC tower accounted for 87% of annual P
361 recorded at the site during the study period (Figure 6). Overall, the simulated annual ET_a at all the
362 TP and CRNP locations is comparable to the annual ET_a measured by the EC tower, except during
363 2012 (Table 7), in which a severe drought occurred in the region. One explanation is that the plants
364 extract more water from deeper layers under extreme drought conditions than what we defined as a
365 maximum rooting depth (150 cm for maize and 120 cm for soybean) for the model, thus limiting
366 the VZM ability to estimate ET_a accurately during the drought year (2012). In fact, based on the
367 EC ET_a measurements at the study site, there was just 8.18% reduction in annual ET_a in 2012 than

368 the average of the other years (2007-2011), while there were 29.58% and 35.75% reduction in
369 annual simulated ET_a values respectively in upscaled TP and CRNP. This shows that although
370 2012 was a very dry year, the plants probably found most of the needed water by extracting water
371 from deeper soil reservoirs. As previously mentioned we defined a maximum rooting depth for the
372 model that could greatly impact the results. To further illustrate this point, a sensitivity analysis
373 was performed on the maximum rooting depth and presented in the following section. However,
374 we note that given the fact that EC ET_a estimation can have up to 20% uncertainty (Massman and
375 Lee, 2002, and Hollineger and Richardson, 2005), and accounting for the natural spatial variability
376 of ET_a due to soil texture and root depth growth uncertainties, the various ET_a estimation
377 techniques performed fairly well. In fact, it is difficult to identify which ET_a estimation method is
378 the most accurate method. These results are consistent with the concept of equifinality in
379 hydrologic modeling given the complexity of natural systems (Beven and Freer, 2001). Moreover,
380 the findings here are consistent with Nearing et al. (2016) that show information lost in model
381 parameters greatly affects the soil moisture comparisons against a benchmark. However, soil
382 parameterization was less important in the loss of information for the comparisons of ET /latent
383 energy against a benchmark. Fully resolving these issues remains a key challenge to the land
384 surface modeling community and the model's ability to make accurate predictions (Best 2015).
385 The following section provides a detailed sensitivity analysis of the soil hydraulic parameters and
386 root depth growth functions in order to begin to understand the sources of error in estimating ET_a
387 from SWC monitoring networks.

388

389 **3.3 Sensitivity analysis of soil hydraulic parameters and rooting depth**

390 In this research we compared simulated ET_a with the measured EC ET_a . As expected some
391 discrepancies between simulated and measured ET_a values existed. In order to begin to understand
392 the key sources of error we performed a set of sensitivity analysis experiments on the estimated
393 soil hydraulic parameters. Building on Wang et al. (2009b), a sensitivity analysis for a single
394 homogeneous soil layer (6 parameters) and a 4-layer soil profile (24 parameters) was performed
395 over the study period (2007–2012). Here we performed a preliminary sensitivity analysis by
396 changing a single soil hydraulic parameter one at a time while keeping the other parameters
397 constant (i.e. at the average value). Figure 10 illustrates the sensitivity results on simulated ET_a ,
398 indicating the soil hydraulic parameters have a range of sensitivities with tortuosity (l) being the
399 least. We found that n and α were the most sensitive, particularly in the shallowest soil layer. This
400 sensitivity to the shallowest soil layer provides an opportunity to use the CRNP observations,
401 particularly in the early growing season (i.e. when evaporation dominates latent energy flux), to
402 help constrain estimates of n and α . As the crop continues to develop (and transpiration contributes
403 a relatively larger component of latent energy) additional information about deeper soil layers
404 should be used to estimate soil hydraulic parameters or perform data assimilation. Moreover, the
405 CRNP may be useful in helping constrain and parameterize soil hydraulic functions in simpler
406 evaporation models widely used in remote sensing (c.f. Allen et al. 2007) and crop modeling (c.f.
407 Allen et al. 1998).

408 Following the sensitivity analysis, we repeated the optimization experiment using only α , n ,
409 K_s , and used model default estimates for the other parameters in each layer. We found that the
410 RMSE values were significantly higher (1.511 vs. 0.911 mm/day) than when considering all 24
411 parameters. We suspect that given the high correlation between soil hydraulic parameters (Carsel
412 and Parrish 1988), that fixing certain parameters leads to a degradation in overall performance. We

413 suggest further sensitivity analyses, in particular changing multiple parameters simultaneously or
414 using multiple objective functions, be used to fully understand model behavior (c.f. Bastidas et al.
415 1999 and Rosolem et al. 2012).

416 A sensitivity analysis of ET_a by varying rooting depth is summarized in Figure 11. As
417 would be expected with increasing rooting depth, higher ET_a occurred. In addition, Figure 11
418 illustrates a decreasing RMSE against EC observations for up to 200% increases. Again it is
419 unclear if the EC observations are biased high or in fact rooting depths are much greater than
420 typically considered in these models. The high observed EC values in the drought year of 2012
421 indicate that roots likely uptake water from below the 1 m observations. Certainly the results
422 shown here further indicate the importance of root water uptake parameters in VZMs and LSMs,
423 even in homogeneous annual cropping systems. While beyond the scope of this paper we refer the
424 reader to the growing literature on the importance of root water uptake parameters on hydrologic
425 fluxes (c.f. Schymanski et al. 2008 and Guswa 2012).

426

427 **3.4 Applications and limitations of the vadose zone modeling framework**

428 Given its simplicity and widespread availability of ground data, ET_r and Kc values are
429 often used in a wide variety of applications to estimate ET_p and thus approximate ET_a . It is well
430 known that SWC is a limiting factor affecting the assumption that $ET_p \sim ET_a$. On the other hand,
431 we know that SWC observations are local in nature and not necessarily representative of ET_a
432 footprint estimates. The key questions are: what is the value of SWC observations, how many
433 profiles do we need to install in a footprint, and at which depths to constrain estimates of fluxes?
434 The well instrumented and long-term study presented here allows us to start to answer these key

435 questions. First we find that ET_p has an average annual value of 1064.9 mm as compared to EC at
436 612.5 mm (Table 7). By including individual SWC profiles (TP 1 to 4) and the CRNP in the VZM
437 framework we are able to constrain our estimate of ET_a to between 525.3 and 643.1 mm and
438 reduce ET_a RMSE from 1.992 mm/day to around 1 mm/day (Table 6). In addition, a range of soil
439 hydraulic parameters for each depth and spatially averaged top layer can be estimated to help
440 better constrain recharge fluxes simultaneously. Given the principle of equifinality in hydrologic
441 systems, the VZM framework may lead to equally reasonable estimates of parameters which is a
442 limitation of the method and LSMs in general. Based on our sensitivity analysis (Figure 10) the
443 key parameters of α , n may greatly affect ET_a .

444 Although sparsely distributed, widespread state, national, and global meteorological
445 observations paired with SWC profiles (Xia et al. 2015) and the VZM framework provide an
446 opportunity to better constrain ET_a and local soil hydraulic functions. Moreover, where multiple
447 SWC profile information is available a range of ET_a and soil hydraulic parameters can be
448 estimated and thus considered in LSM data assimilation frameworks. The combination of basic
449 metrological observations with a CRNP in the VZM framework further allows for estimates of
450 upscaled soil hydraulic parameters with similar estimates of ET_a as found with individual SWC
451 profiles. Moving forward, combining CRNP with deeper SWC observations from point sensors
452 seems to be a reasonable strategy in order to average the inherent SWC variability in the near
453 surface yet provide SWC constraints at depth, particularly as annual crops develop over the
454 growing season.

455

456 **4. Conclusions**

457 In this study the feasibility of using inverse vadose zone modeling for field scale ET_a
458 estimation was explored at an agricultural site in eastern Nebraska. Both point SWC sensors (TP)
459 and area-average techniques (CRNP) were explored. This methodology has been successfully used
460 for estimates of groundwater recharge but it was critical to assess the performance of other
461 components of the water balance such as ET_a . The results indicate reasonable estimates of daily
462 and annual ET_a but with varied soil hydraulic function parameterizations. The varied soil hydraulic
463 parameters were expected given the heterogeneity of soil texture at the site and consistent with the
464 principle of equifinality in hydrologic systems. We note that while this study focused on one
465 particular site, the framework can be easily applied to other networks of SWC monitoring across
466 the globe (Xia et al., 2015). The value added products of groundwater recharge and ET_a flux from
467 the SWC monitoring networks will provide additional and more robust benchmarks for the
468 validation of LSM that continue to improve their forecast skill.

469

470 **5. Data availability**

471 The climatic and EC data used in this research can be found at <http://ameriflux.lbl.gov/>.
472 The TP SWC and LAI data in the study site are provided by Dr. Andrew Suyker and CRNP SWC
473 are provided by Dr. Trenton E. Franz and both sets of data can be requested directly from the
474 authors. The US soil taxonomy information is provided by Soil Survey Staff and is available
475 online at <http://websoilsurvey.nrcs.usda.gov/> (accessed in July, 2016). The remaining datasets are
476 provided in the supplemental material associated with this paper.

477

478 **Acknowledgments**

479 This research is supported financially by the Daugherty Water for Food Global Institute at
480 the University of Nebraska, NSF EPSCoR FIRST Award, the Cold Regions Research Engineering
481 Laboratory through the Great Plains CESU, and an USGS104b grant. We sincerely appreciate the
482 support and the use of facilities and equipment provided by the Center for Advanced Land
483 Management Information Technologies, School of Natural Resources and data from Carbon
484 Sequestration Program, the University of Nebraska-Lincoln. TEF would like to thank Eric Wood
485 for his inspiring research and teaching career. No doubt the skills TEF learned while at Princeton
486 in formal course work, seminars, and discussions with Eric will serve him well in his own career.

487 **References**

- 488 Allen, R. G., Pereira, L. S., Raes, D., & Smith, M. (1998). Crop evapotranspiration-guidelines for
489 computing crop water requirements-FAO irrigation and drainage paper 56. FAO, Rome,
490 300(9), D05109.
- 491 Allen, R. G., Tasumi, M., & Trezza, R. (2007). Satellite-based energy balance for mapping
492 evapotranspiration with internalized calibration (METRIC)—Model. *Journal of Irrigation and*
493 *Drainage Engineering*, 133(4), 380-394.
- 494 Anayah, F. M., & Kaluarachchi, J. J. (2014). Improving the complementary methods to estimate
495 evapotranspiration under diverse climatic and physical conditions. *Hydrology and Earth*
496 *System Sciences*, 18(6), 2049-2064.
- 497 Andreasen, M., Andreasen, L. A., Jensen, K. H., Sonnenborg, T. O., & Bircher, S. (2013).
498 Estimation of regional groundwater recharge using data from a distributed soil moisture
499 network. *Vadose Zone Journal*, 12(3)
- 500 ASCE – EWRI. (2005). The ASCE Standardized reference evapotranspiration equation. ASCE-
501 EWRI Standardization of Reference Evapotranspiration Task Comm. Report, ASCE
502 Bookstore, ISBN 078440805, Stock Number 40805, 216 pages.
- 503 Baatz, R., Bogaen, H., Franssen, H. H., Huisman, J., Qu, W., Montzka, C., et al. (2014).
504 Calibration of a catchment scale cosmic-ray probe network: A comparison of three
505 parameterization methods. *Journal of Hydrology*, 516, 231-244.
- 506 Baldocchi, D. D., Hincks, B. B., & Meyers, T. P. (1988). Measuring biosphere-atmosphere
507 exchanges of biologically related gases with micrometeorological methods. *Ecology*, 1331-
508 1340.
- 509 Baldocchi, D., Falge, E., Gu, L., & Olson, R. (2001). FLUXNET: A new tool to study the temporal
510 and spatial variability of ecosystem-scale carbon dioxide, water vapor, and energy flux
511 densities. *Bulletin of the American Meteorological Society*, 82(11), 2415.

512 Bastidas, L. A., H. V. Gupta, S. Sorooshian, W. J. Shuttleworth, and Z. L. Yang (1999), Sensitivity
513 analysis of a land surface scheme using multicriteria methods, *J. Geophys. Res.-Atmos.*,
514 104(D16), 19481-19490. doi:10.1029/1999jd900155.

515 Best, M., Abramowitz, G., Johnson, H., Pitman, A., Balsamo, G., Boone, A., et al. (2015). The
516 plumbing of land surface models: Benchmarking model performance. *Journal of*
517 *Hydrometeorology*, 16(3), 1425-1442.

518 Beven, K., & Freer, J. (2001). Equifinality, data assimilation, and uncertainty estimation in
519 mechanistic modelling of complex environmental systems using the GLUE methodology.
520 *Journal of Hydrology*, 249(1), 11-29.

521 Bogena, H., Huisman, J., Baatz, R., Hendricks Franssen, H., & Vereecken, H. (2013). Accuracy of
522 the cosmic-ray soil water content probe in humid forest ecosystems: The worst case scenario.
523 *Water Resources Research*, 49(9), 5778-5791.

524 Carsel, R. F., & Parrish, R. S. (1988). Developing joint probability distributions of soil water
525 retention characteristics. *Water Resources Research*, 24(5), 755-769.

526 Chaney, N. W., Wood, E. F., McBratney, A. B., Hempel, J. W., Nauman, T. W., Brungard, C. W.,
527 et al. (2016). POLARIS: A 30-meter probabilistic soil series map of the contiguous United
528 States. *Geoderma*, 274, 54-67.

529 Chemin, Y., & Alexandridis, T. (2001). Improving spatial resolution of ET seasonal for irrigated
530 rice in Zhanghe, china. Paper Presented at the 22nd Asian Conference on Remote Sensing, 5.
531 pp. 9.

532 Desilets, D., & Zreda, M. (2013). Footprint diameter for a cosmic-ray soil moisture probe: Theory
533 and monte carlo simulations. *Water Resources Research*, 49(6), 3566-3575.

534 Entekhabi, D., E. G. Njoku, P. E. O'Neill, K. H. Kellogg, W. T. Crow, W. N. Edelstein, J. K.
535 Entin, S. D. Goodman, T. J. Jackson, J. Johnson, J. Kimball, J. R. Piepmeier, R. D. Koster, N.
536 Martin, K. C. McDonald, M. Moghaddam, S. Moran, R. Reichle, J. C. Shi, M. W. Spencer, S.

537 W. Thurman, L. Tsang, and J. Van Zyl (2010), The Soil Moisture Active Passive (SMAP)
538 Mission, Proc. IEEE, 98(5), 704-716. doi:10.1109/jproc.2010.2043918.

539 Feddes, R. A., Kowalik, P. J., & Zaradny, H. (1978). Simulation of field water use and crop yield.
540 Centre for Agricultural Publishing and Documentation.

541 Franz, T. E., Wahbi, A., Vreugdenhil, M., Weltin, G., Heng, L., Oismueller, M., et al. (2016).
542 Using cosmic-ray neutron probes to monitor landscape scale soil water content in mixed land
543 use agricultural systems. Applied and Environmental Soil Science, 2016.

544 Franz, T. E., Wang, T., Avery, W., Finkenbiner, C., & Brocca, L. (2015). Combined analysis of
545 soil moisture measurements from roving and fixed cosmic ray neutron probes for multiscale
546 real-time monitoring. Geophysical Research Letters, 42(9), 3389-3396.

547 Franz, T. E., Zreda, M., Ferre, T., Rosolem, R., Zweck, C., Stillman, S., et al. (2012).
548 Measurement depth of the cosmic ray soil moisture probe affected by hydrogen from various
549 sources. Water Resources Research, 48(8).

550 Galleguillos, M., Jacob, F., Prévot, L., Lagacherie, P., & Liang, S. (2011). Mapping daily
551 evapotranspiration over a Mediterranean vineyard watershed. Geoscience and Remote
552 Sensing Letters, IEEE, 8(1), 168-172.

553 Glenn, E. P., Huete, A. R., Nagler, P. L., Hirschboeck, K. K., & Brown, P. (2007). Integrating
554 remote sensing and ground methods to estimate evapotranspiration. Critical Reviews in Plant
555 Sciences, 26(3), 139-168.

556 Guswa, A. J. (2012), Canopy vs. Roots: Production and Destruction of Variability in Soil Moisture
557 and Hydrologic Fluxes, Vadose Zone Journal, 11(3). doi:10.2136/vzj2011.0159.

558 Hawdon, A., McJannet, D., & Wallace, J. (2014). Calibration and correction procedures for
559 cosmic-ray neutron soil moisture probes located across Australia. Water Resources Research,
560 50(6), 5029-5043.

- 561 Hollinger, D. Y., & Richardson, A. D. (2005). Uncertainty in eddy covariance measurements and
562 its application to physiological models. *Tree Physiology*, 25(7), 873-885.
- 563 Hopmans, J.W., Šimunek, J., 1999. Review of inverse estimation of soil hydraulic properties. In:
564 van Genuchten, M.Th. Leij, F.J., Wu, L. (Eds.), *Proceedings of the International Workshop*
565 *Characterization and Measurement of Hydraulic Properties of Unsaturated Porous Media*.
566 University of California, Riverside, 643–659. Irmak, S. (2010). Nebraska water and energy
567 flux measurement, modeling, and research network (NEBFLUX). *Transactions of the*
568 *ASABE*, 53(4), 1097-1115. Irmak, S. (2010). Nebraska water and energy flux measurement,
569 modeling, and research network (NEBFLUX). *Transactions of the ASABE*, 53(4), 1097-1115.
- 570 Izadifar, Z., & Elshorbagy, A. (2010). Prediction of hourly actual evapotranspiration using neural
571 networks, genetic programming, and statistical models. *Hydrological Processes*, 24(23), 3413-
572 3425.
- 573 Jiménez-Martínez, J., Skaggs, T., Van Genuchten, M. T., & Candela, L. (2009). A root zone
574 modelling approach to estimating groundwater recharge from irrigated areas. *Journal of*
575 *Hydrology*, 367(1), 138-149.
- 576 Kalfas, J. L., Xiao, X., Vanegas, D. X., Verma, S. B., & Suyker, A. E. (2011). Modeling gross
577 primary production of irrigated and rain-fed maize using MODIS imagery and CO₂ flux
578 tower data. *Agricultural and Forest Meteorology*, 151(12), 1514-1528.
- 579 Kjaersgaard, J., Allen, R., Trezza, R., Robinson, C., Oliveira, A., Dhungel, R., et al. (2012). Filling
580 satellite image cloud gaps to create complete images of evapotranspiration. *IAHS-AISH*
581 *Publication*, 102-105.
- 582 Köhli, M., Schrön, M., Zreda, M., Schmidt, U., Dietrich, P., & Zacharias, S. (2015). Footprint
583 characteristics revised for field-scale soil moisture monitoring with cosmic-ray neutrons.
584 *Water Resources Research*, 51(7), 5772-5790.

585 Li, Z., Tang, R., Wan, Z., Bi, Y., Zhou, C., Tang, B., et al. (2009). A review of current
586 methodologies for regional evapotranspiration estimation from remotely sensed data. *Sensors*,
587 9(5), 3801-3853.

588 Lv, L., Franz, T. E., Robinson, D. A., & Jones, S. B. (2014). Measured and modeled soil moisture
589 compared with cosmic-ray neutron probe estimates in a mixed forest. *Vadose Zone Journal*,
590 13(12)

591 Maidment, D. R. (1992). *Handbook of hydrology*. McGraw-Hill Inc.

592 Massman, W., & Lee, X. (2002). Eddy covariance flux corrections and uncertainties in long-term
593 studies of carbon and energy exchanges. *Agricultural and Forest Meteorology*, 113(1), 121-
594 144.

595 McMaster, G. S., & Wilhelm, W. (1997). Growing degree-days: One equation, two interpretations.
596 *Agricultural and Forest Meteorology*, 87(4), 291-300.

597 Min, L., Shen, Y., & Pei, H. (2015). Estimating groundwater recharge using deep vadose zone data
598 under typical irrigated cropland in the piedmont region of the north china plain. *Journal of*
599 *Hydrology*, 527, 305-315.

600 Mualem, Y. (1976). A new model for predicting the hydraulic conductivity of unsaturated porous
601 media. *Water Resources Research*, 12(3), 513-522.

602 Nearing, G. S., Mocko, D. M., Peters-Lidard, C. D., Kumar, S. V., & Xia, Y. (2016).
603 Benchmarking NLDAS-2 soil moisture and evapotranspiration to separate uncertainty
604 contributions. *Journal of Hydrometeorology*, 17(3), 745-759.

605 Renzullo, L. J., Van Dijk, A., Perraud, J., Collins, D., Henderson, B., Jin, H., et al. (2014).
606 Continental satellite soil moisture data assimilation improves root-zone moisture analysis for
607 water resources assessment. *Journal of Hydrology*, 519, 2747-2762.

608 Ries, F., Lange, J., Schmidt, S., Puhlmann, H., & Sauter, M. (2015). Recharge estimation and soil
609 moisture dynamics in a Mediterranean, semi-arid karst region. *Hydrology and Earth System
610 Sciences*, 19(3), 1439-1456.

611 Ritter, A., Hupet, F., Muñoz-Carpena, R., Lambot, S., & Vanclooster, M. (2003). Using inverse
612 methods for estimating soil hydraulic properties from field data as an alternative to direct
613 methods. *Agricultural Water Management*, 59(2), 77-96.

614 Rosolem, R., H. V. Gupta, W. J. Shuttleworth, X. B. Zeng, and L. G. G. de Goncalves (2012), A
615 fully multiple-criteria implementation of the Sobol' method for parameter sensitivity analysis,
616 *J. Geophys. Res.-Atmos.*, 117. doi:10.1029/2011jd016355.

617 Schaap, M. G., Leij, F. J., & Van Genuchten, M. T. (2001). Rosetta: A computer program for
618 estimating soil hydraulic parameters with hierarchical pedotransfer functions. *Journal of
619 Hydrology*, 251(3), 163-176.

620 Schymanski, S. J., M. Sivapalan, M. L. Roderick, J. Beringer, and L. B. Hutley (2008), An
621 optimality-based model of the coupled soil moisture and root dynamics, *Hydrology and Earth
622 System Sciences*, 12(3), 913-932.

623 Senay, G. B., Budde, M. E., & Verdin, J. P. (2011). Enhancing the simplified surface energy
624 balance (SSEB) approach for estimating landscape ET: Validation with the METRIC model.
625 *Agricultural Water Management*, 98(4), 606-618.

626 Šimunek, J., Šejna, M., Saito, H., Sakai, M., van Genuchten, M.T. (2013). The HYDRUS-1D
627 Software Package for Simulating the One-Dimensional Movement of Water, Heat, and Multiple
628 Solutes in Variably-Saturated Media, Version 4.17. Department of Environmental Sciences,
629 University of California Riverside, Riverside, California, USA, 307 pp.

630 Soil Survey Staff, Natural Resources Conservation Service, United States Department of
631 Agriculture. Web Soil Survey. Available online at <http://websoilsurvey.nrcs.usda.gov/>.
632 Accessed in July, 2016.

- 633 Stoy, P. (2012). Evapotranspiration and energy flux observations from a global tower network with
634 a critical analysis of uncertainties. AGU Fall Meeting Abstracts, 1. pp. 06.
- 635 Suyker, A., Verma, S., Burba, G., Arkebauer, T., Walters, D., & Hubbard, K. (2004). Growing
636 season carbon dioxide exchange in irrigated and rainfed maize. *Agricultural and Forest
637 Meteorology*, 124(1), 1-13.
- 638 Suyker, A. E., & Verma, S. B. (2008). Interannual water vapor and energy exchange in an irrigated
639 maize-based agroecosystem. *Agricultural and Forest Meteorology*, 148(3), 417-427.
- 640 Suyker, A. E., & Verma, S. B. (2009). Evapotranspiration of irrigated and rainfed maize–soybean
641 cropping systems. *Agricultural and Forest Meteorology*, 149(3), 443-452.
- 642 Suyker, A. E., Verma, S. B., Burba, G. G., & Arkebauer, T. J. (2005). Gross primary production
643 and ecosystem respiration of irrigated maize and irrigated soybean during a growing season.
644 *Agricultural and Forest Meteorology*, 131(3), 180-190.
- 645 Suyker, A. E., Verma, S. B., Burba, G. G., & Arkebauer, T. J. (2005). Gross primary production
646 and ecosystem respiration of irrigated maize and irrigated soybean during a growing season.
647 *Agricultural and Forest Meteorology*, 131(3), 180-190.
- 648 Turkeltaub, T., Kurtzman, D., Bel, G., & Dahan, O. (2015). Examination of groundwater recharge
649 with a calibrated/validated flow model of the deep vadose zone. *Journal of Hydrology*, 522,
650 618-627.
- 651 Twarakavi, N. K. C., Šimůnek, J., & Seo, S. (2008). Evaluating interactions between groundwater
652 and vadose zone using the HYDRUS-based flow package for MODFLOW. *Vadose Zone
653 Journal*, 7(2), 757-768.
- 654 van Genuchten, M. T. (1980). A closed-form equation for predicting the hydraulic conductivity of
655 unsaturated soils. *Soil Science Society of America Journal*, 44(5), 892-898.

- 656 Verma, S. B., Dobermann, A., Cassman, K. G., Walters, D. T., Knops, J. M., Arkebauer, T. J., et
657 al. (2005). Annual carbon dioxide exchange in irrigated and rainfed maize-based
658 agroecosystems. *Agricultural and Forest Meteorology*, 131(1), 77-96.
- 659 Wang, T., & Franz, T. E. (2015). Field observations of regional controls of soil hydraulic
660 properties on soil moisture spatial variability in different climate zones. *Vadose Zone Journal*,
661 14(8)
- 662 Wang, T., Franz, T. E., Yue, W., Szilagyi, J., Zlotnik, V. A., You, J., et al. (2016). Feasibility
663 analysis of using inverse modeling for estimating natural groundwater recharge from a large-
664 scale soil moisture monitoring network. *Journal of Hydrology*, 533, 250-265.
- 665 Wang, T., Franz, T. E., & Zlotnik, V. A. (2015). Controls of soil hydraulic characteristics on
666 modeling groundwater recharge under different climatic conditions. *Journal of Hydrology*,
667 521, 470-481.
- 668 Wang, T., Istanbuluoglu, E., Lenters, J., & Scott, D. (2009a). On the role of groundwater and soil
669 texture in the regional water balance: An investigation of the Nebraska sand hills, USA. *Water*
670 *Resources Research*, 45(10)
- 671 Wang, T., Zlotnik, V. A., Šimunek, J., & Schaap, M. G. (2009b). Using pedotransfer functions in
672 vadose zone models for estimating groundwater recharge in semiarid regions. *Water*
673 *Resources Research*, 45(4)
- 674 Wolf, A., Saliendra, N., Akshalov, K., Johnson, D. A., & Laca, E. (2008). Effects of different eddy
675 covariance correction schemes on energy balance closure and comparisons with the modified
676 bowen ratio system. *Agricultural and Forest Meteorology*, 148(6), 942-952.
- 677 Wood, E. F., Roundy, J. K., Troy, T. J., Van Beek, L., Bierkens, M. F., Blyth, E., et al. (2011).
678 Hyperresolution global land surface modeling: Meeting a grand challenge for monitoring
679 earth's terrestrial water. *Water Resources Research*, 47(5)

- 680 Wösten, J., Pachepsky, Y. A., & Rawls, W. (2001). Pedotransfer functions: Bridging the gap
681 between available basic soil data and missing soil hydraulic characteristics. *Journal of*
682 *Hydrology*, 251(3), 123-150.
- 683 Xia, Y., Ek, M. B., Wu, Y., Ford, T., & Quiring, S. M. (2015). Comparison of NLDAS-2
684 simulated and NASMD observed daily soil moisture. part I: Comparison and analysis. *Journal*
685 *of Hydrometeorology*, 16(5), 1962-1980.
- 686 Xie, Y., Sha, Z., & Yu, M. (2008). Remote sensing imagery in vegetation mapping: A review.
687 *Journal of Plant Ecology*, 1(1), 9-23.
- 688 Yang, H., Dobermann, A., Cassman, K. G., & Walters, D. T. (2004). Hybrid-maize. A Simulation
689 Model for Corn Growth and Yield. Nebraska Cooperative Extension CD, 9.
- 690 Yang, W., Yang, L., & Merchant, J. (1997). An assessment of AVHRR/NDVI-ecoclimatological
691 relations in Nebraska, USA. *International Journal of Remote Sensing*, 18(10), 2161-2180.
- 692 Zhang, L., Dawes, W., & Walker, G. (2001). Response of mean annual evapotranspiration to
693 vegetation changes at catchment scale. *Water Resources Research*, 37(3), 701-708.
- 694 Zhang, Z., Tian, F., Hu, H., & Yang, P. (2014). A comparison of methods for determining field
695 evapotranspiration: Photosynthesis system, sap flow, and eddy covariance. *Hydrology and*
696 *Earth System Sciences*, 18(3), 1053-1072.
- 697 Zreda, M., Shuttleworth, W., Zeng, X., Zweck, C., Desilets, D., Franz, T., et al. (2012). COSMOS:
698 The cosmic-ray soil moisture observing system. *Hydrology and Earth System Sciences*,
699 16(11), 4079-4099.
- 700 Zreda, M., Desilets, D., Ferré, T., & Scott, R. L. (2008). Measuring soil moisture content non-
701 invasively at intermediate spatial scale using cosmic-ray neutrons. *Geophysical Research*
702 *Letters*, 35(21).

703

704 **List of Figures**

705 Figure 1. Study site (Mead Rainfed/US-Ne3) location in Nebraska (a) and locations of Eddy-
706 Covariance Tower (EC), Cosmic-Ray Neutron Probe (CRNP), Theta Probes (TPs), and
707 variability of soil texture based on Web Soil Survey data at the study site, 2014 (b). See table 1
708 for soil descriptions.

709 Figure 2. Eddy-Covariance Tower (a) and Cosmic-Ray Neutron Probe (b) Located at the Mead
710 Rainfed (US-Ne3) Site.

711 Figure 3. Daily precipitation (P) and reference evapotranspiration (ET_r) during the calibration
712 (2008–2010) and validation (2011–2012) periods at the Mead Rainfed (US-Ne3) Site.

713 Figure 4. Temporal evolution of daily SWC (θ) at different soil depths. The black lines represent
714 daily mean SWC (θ) calculated from TPs in 4 different locations at study site and the blue areas
715 indicate one standard deviation.

716 Figure 5. Time series of daily CRNP and spatial average TP SWC (θ) data.

717 Figure 6. Annual precipitation (P) and annual actual evapotranspiration (ET_a) at the Mead Rainfed
718 (US-Ne3) Site.

719 Figure 7. Daily observed and simulated SWC (θ) during the calibration (2008–2010) and validation
720 (2011–2012) periods at TP 1 location. See supplemental figures for other comparisons.

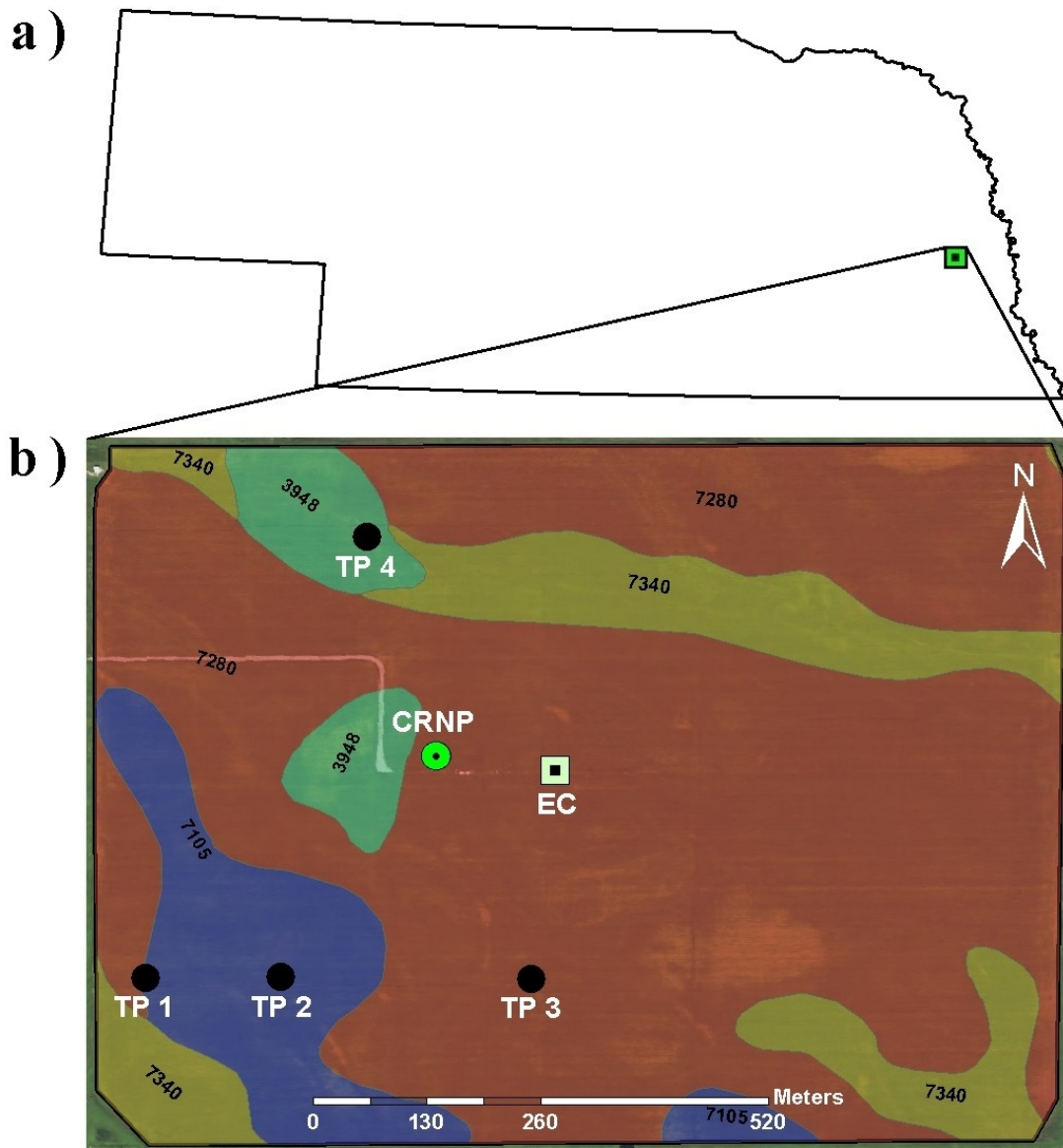
721 Figure 8. Daily observed and simulated SWC (θ) during the calibration (2012–2013) and validation
722 (2014) periods at the location of Cosmic-Ray Neutron probe.

723 Figure 9. Simulated daily ET_a versus Observed daily ET_a in different locations at the study site
724 (2007-2012).

725 Figure 10. Sensitivity Analysis of Effect of Soil Hydraulic Parameters on average annual ET_a
726 values (2007-2012) for a single homogeneous soil layer (6 parameters) and for a 4-layer soil
727 profile (24 parameters).

728 Figure 11. Sensitivity Analysis of Effect of Root Depth on ET_a estimation for a single
729 homogeneous soil layer profile. Note that root depth is in terms of percent depth as it is

730 dynamic over the growing period.

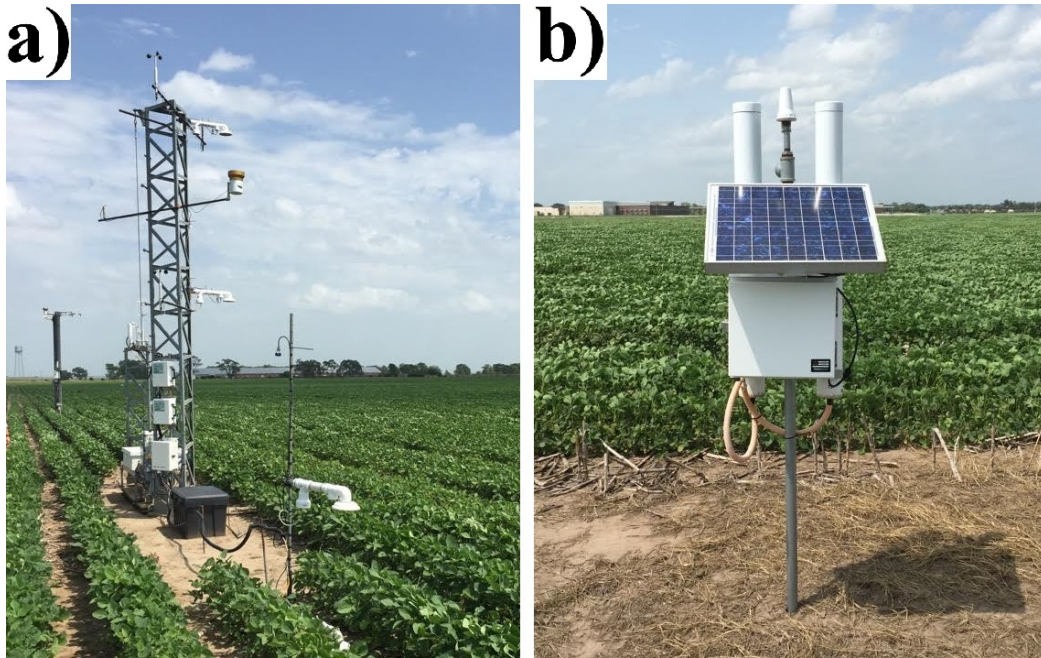


731

732 Figure 1. Study site (Mead Rainfed/US-Ne3) location in Nebraska (a) and locations of Eddy-
 733 Covariance Tower (EC), Cosmic-Ray Neutron Probe (CRNP), Theta Probes (TPs), and
 734 variability of soil texture based on Web Soil Survey data at the study site, 2014 (b). See table 1
 735 for soil descriptions.

736

737

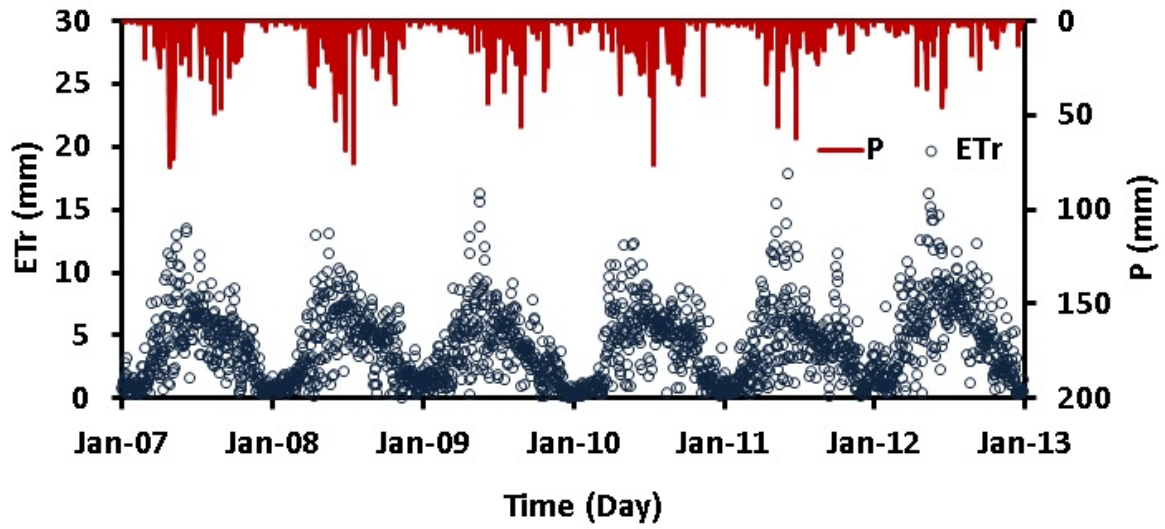


738

739

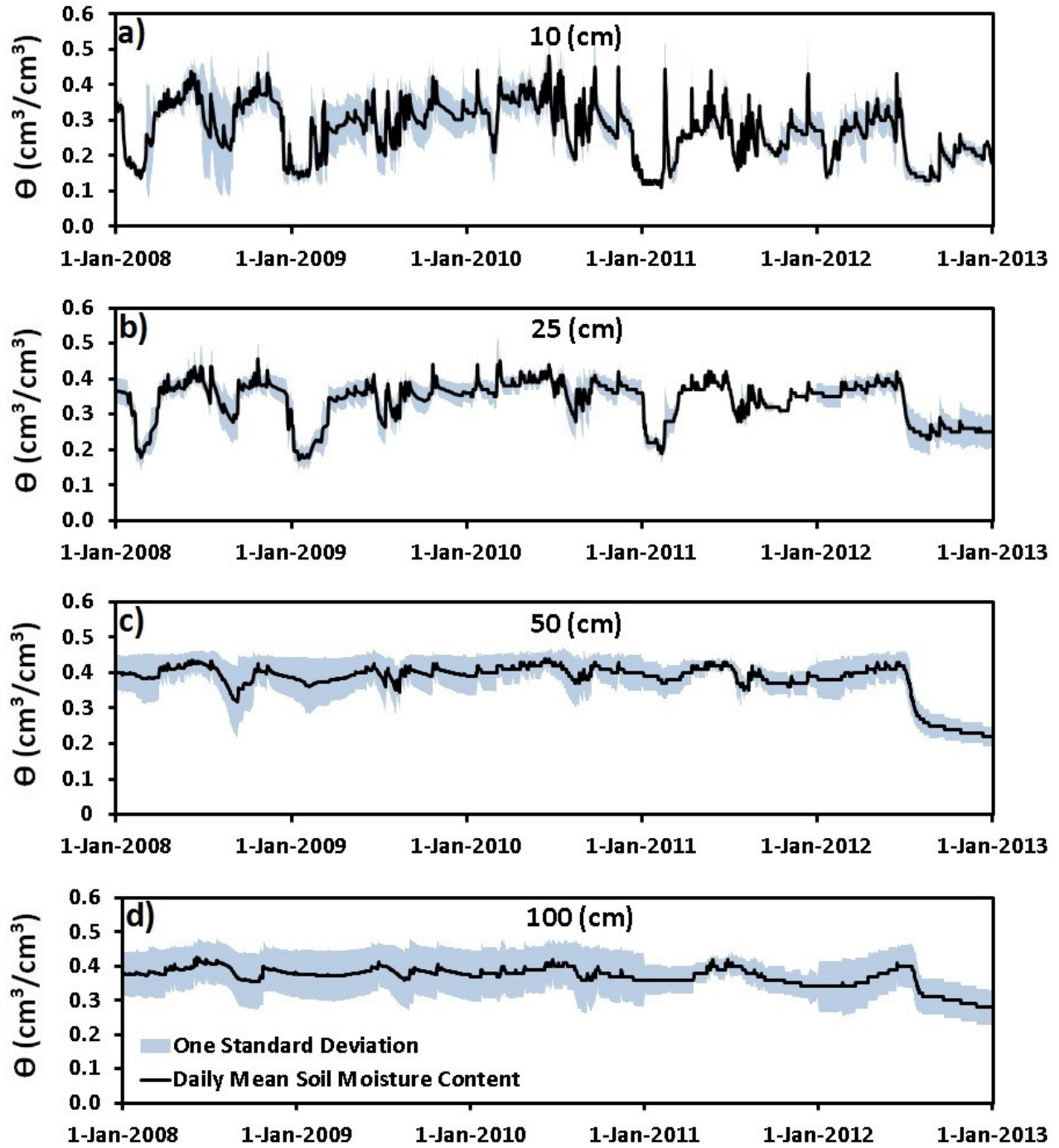
740

Figure 2. Eddy-Covariance Tower (a) and Cosmic-Ray Neutron Probe (b) Located at the Mead Rainfed (US-Ne3) Site.



741
742
743

Figure 3. Daily precipitation (P) and reference evapotranspiration (ET_r) during the calibration (2008–2010) and validation (2011–2012) periods at the Mead Rainfed (US-Ne3) Site.



744

745 Figure 4. Temporal evolution of daily *SWC* (θ) at different soil depths. The black lines represent
 746 daily mean *SWC* (θ) calculated from TPs in 4 different locations at study site and the blue areas
 747 indicate one standard deviation.

748

749

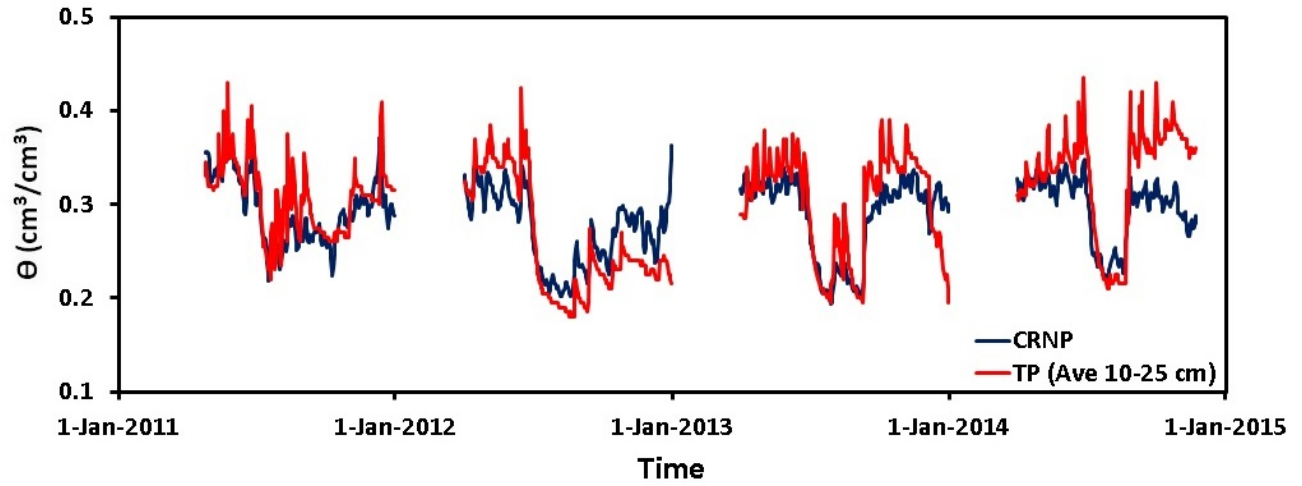
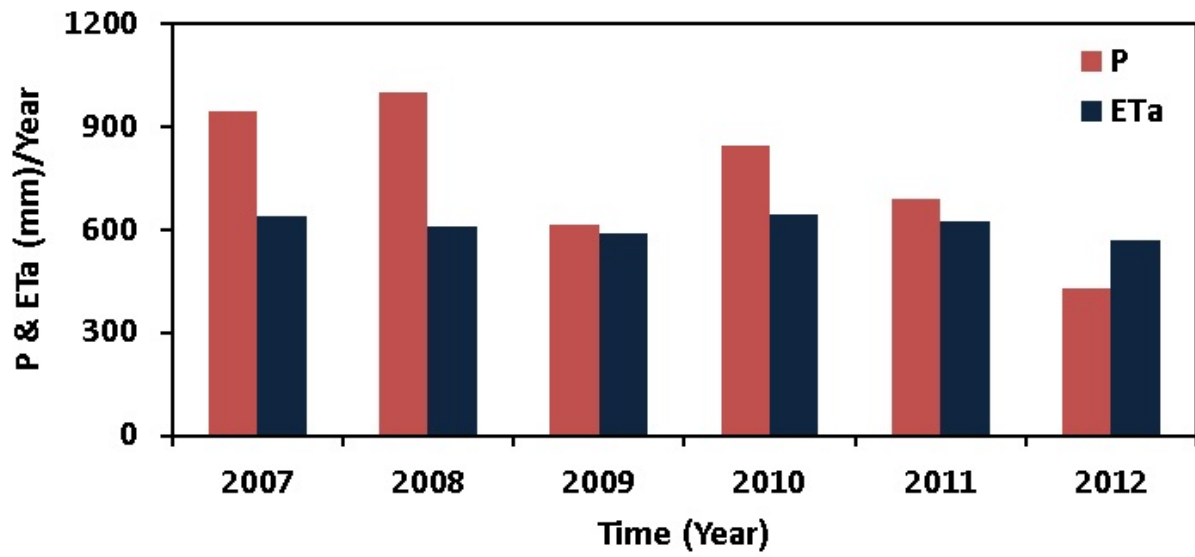


Figure 5. Time series of daily CRNP and spatial average TP *SWC* (θ) data.

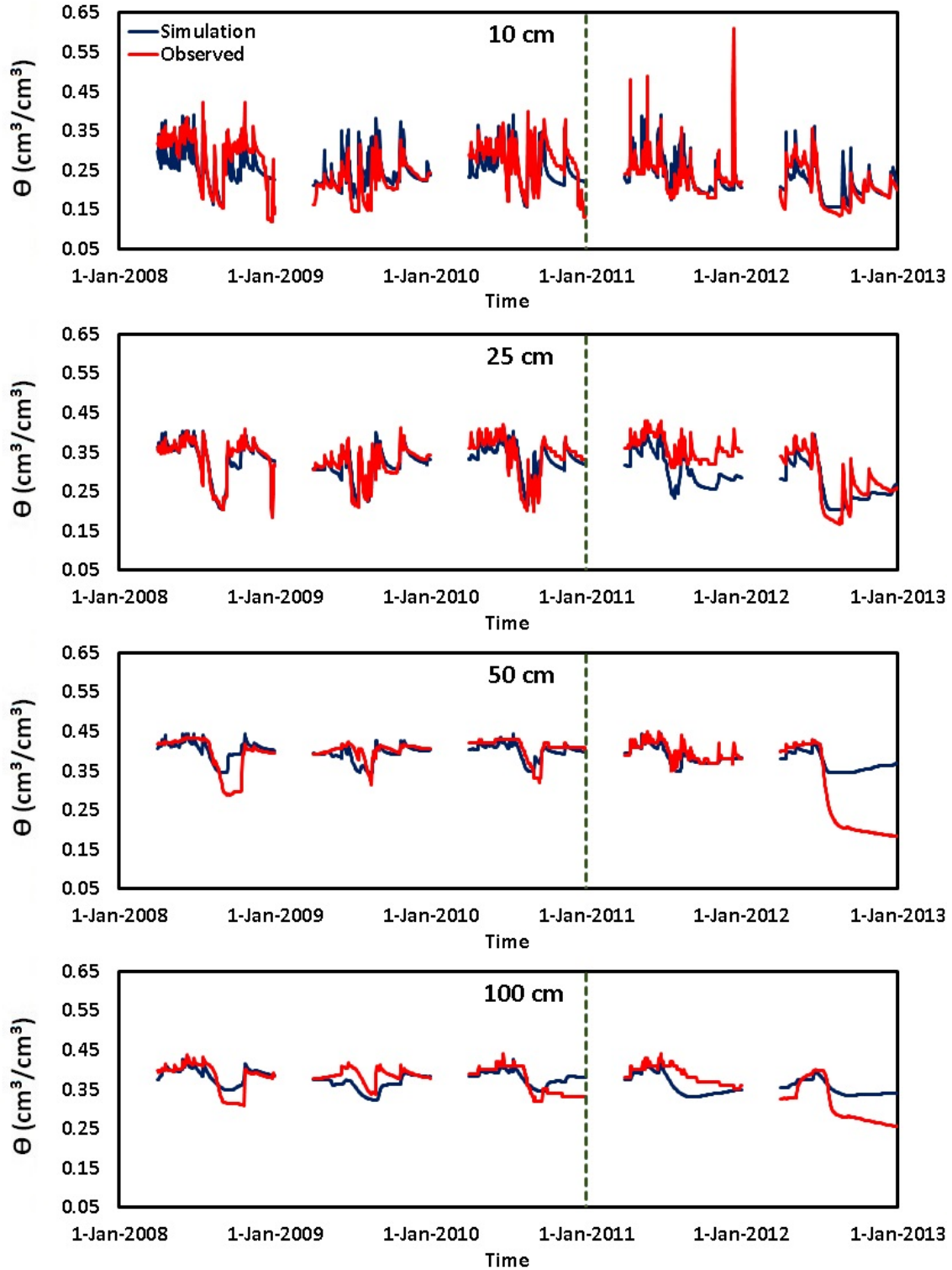
750
 751
 752
 753
 754
 755
 756
 757
 758
 759
 760
 761
 762
 763
 764



765

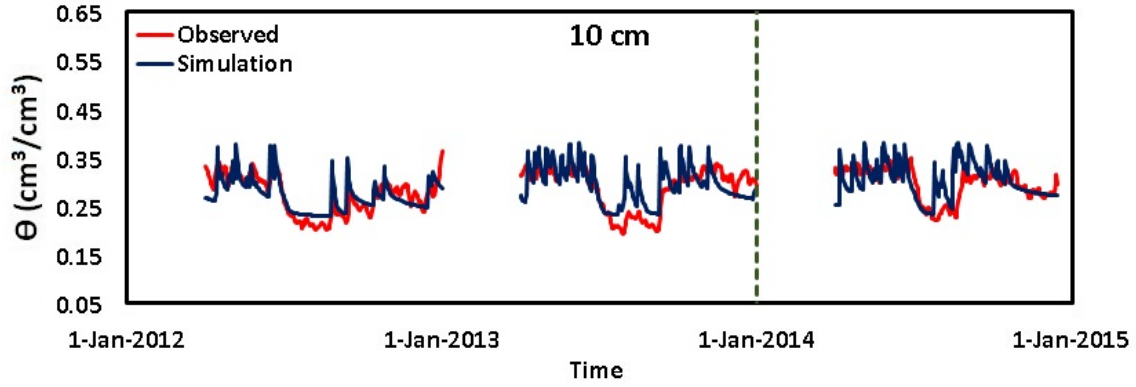
766 Figure 6. Annual precipitation (P) and annual actual evapotranspiration (ET_a) at the Mead Rainfed
 767 (US-Ne3) Site.

768



769

770 Figure 7. Daily observed and simulated *SWC* (θ) during the calibration (2008–2010) and validation
 771 (2011–2012) periods at TP 1 location. See supplemental figures for other comparisons.



772
 773 Figure 8. Daily observed and simulated *SWC* (θ) during the calibration (2012–2013) and validation
 774 (2014) periods at the location of Cosmic-Ray Neutron probe.

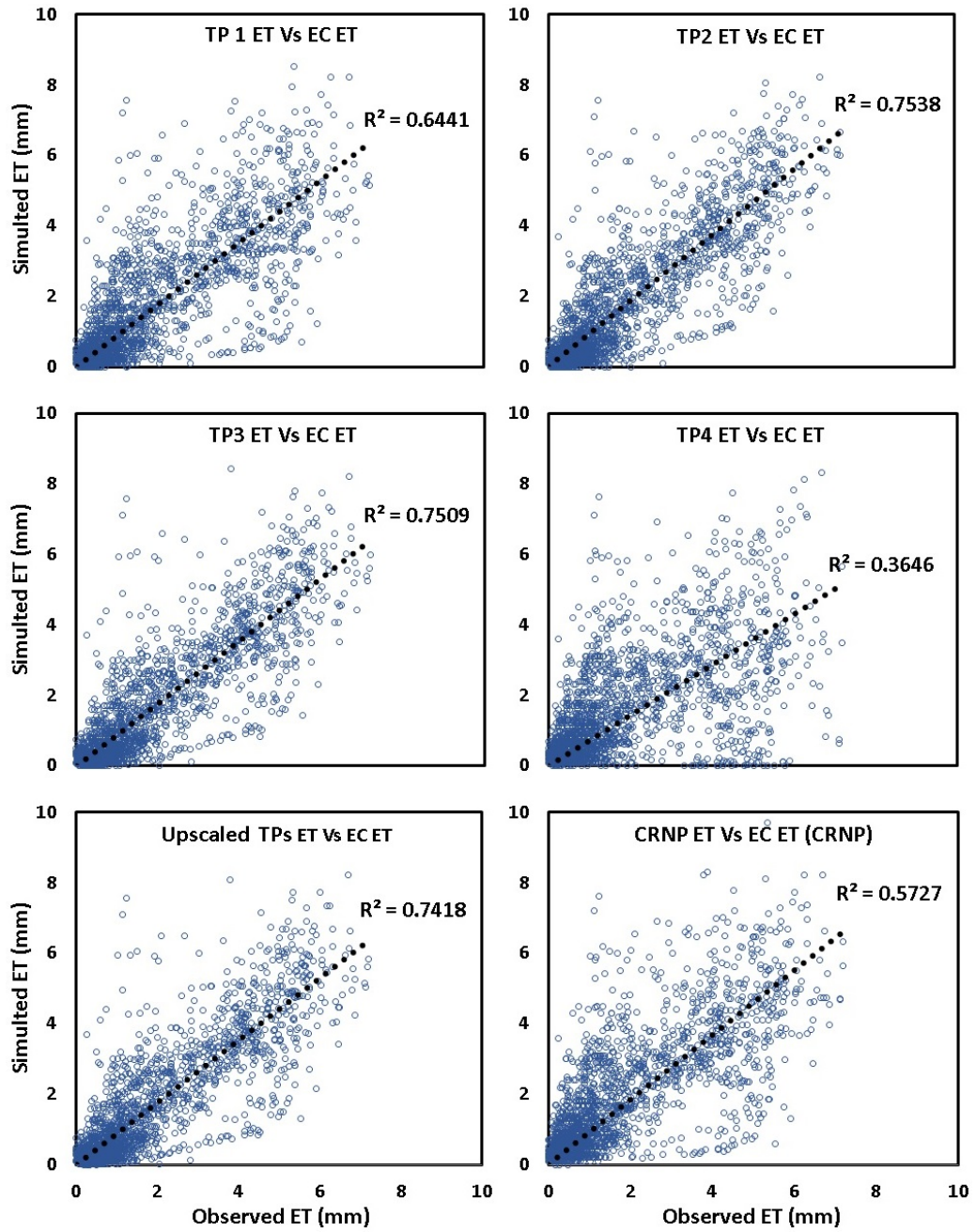
775

776

777

778

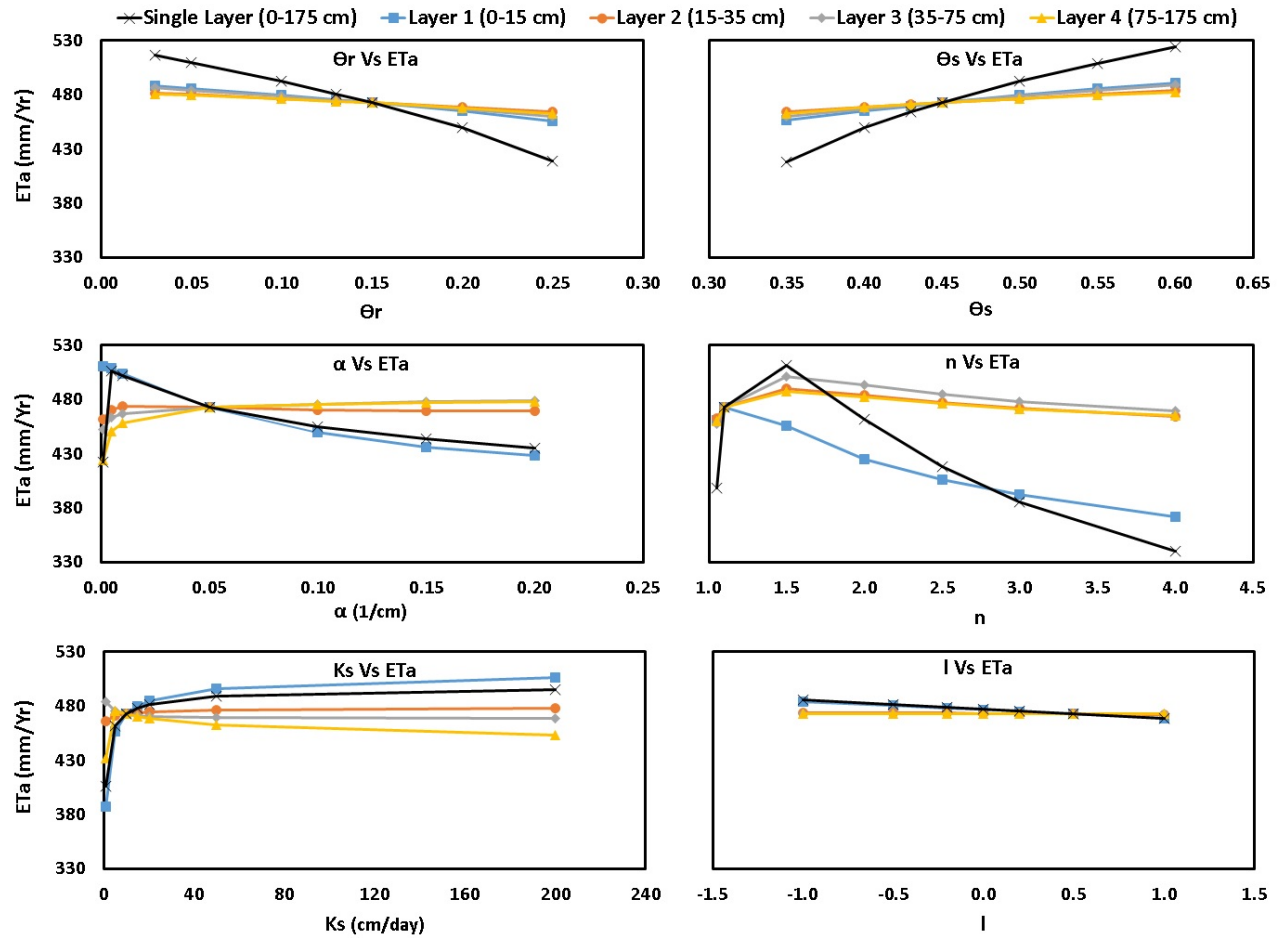
779



780

781 Figure 9. Simulated daily ET_a versus observed daily ET_a at different locations in the study site
 782 (2007-2012).

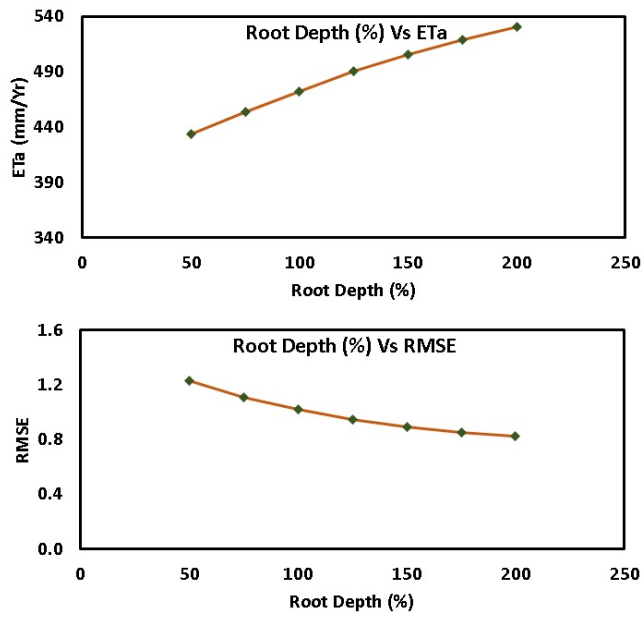
783



784

785 Figure 10. Sensitivity analysis of the effect of soil hydraulic parameters on average annual ET_a
 786 values (2007-2012) for a single homogeneous soil layer (6 parameters) and for a 4-layer soil
 787 profile (24 parameters).

788



789
 790 Figure 11. Sensitivity analysis of root depth on *ETa* estimation for a single homogeneous soil layer
 791 profile. Note that root depth is in terms of percent depth as it is dynamic over the growing period.
 792

- 793
- 794 **List of Tables**
- 795 Table 1. Variability of soil texture in the study field based on Web Soil Survey data
796 (<http://websoilsurvey.sc.egov.usda.gov/App/HomePage.htm>).
- 797 Table 2. Bounds of the van Genuchten parameters used for inverse modeling.
- 798 Table 3. Goodness-of-fit measures for simulated and observed *SWC* data at different depths during
799 the calibration period (2008 to 2010) and validation period (2011-2012) at TPs locations.
- 800 Table 4. Goodness-of-fit measures for simulated and observed *SWC* data during the calibration
801 period (2012 to 2013) and validation period (2014) at CRNP location.
- 802 Table 5. Optimized van Genuchten parameters in different locations at the study site. Note, 95%
803 confidence intervals are in parentheses.
- 804 Table 6. Goodness-of-fit measures for simulated and observed daily ET_a during the simulation
805 period (2007-2012) at study site.
- 806 Table 7. Summary of simulated yearly and average actual evapotranspiration (ET_a) (mm) and
807 observed yearly and average actual evapotranspiration (ET_a) (mm) from Eddy-Covariance
808 tower during 2007 to 2012.
- 809
- 810
- 811
- 812
- 813
- 814

815

816
817

Table 1. Variability of soil texture in the study field based on Web Soil Survey data (<http://websoilsurvey.sc.egov.usda.gov/App/HomePage.htm>).

Map Unit Symbol	Map Unit Name	Clay (%)	Silt (%)	Sand (%)	Hectares in Field	Percent of Field
3948	Fillmore silt loam, terrace, occasionally ponded	41.7	51.0	7.3	3.24	4.9%
7105	Yutan silty clay loam, terrace, 2 to 6 percent slopes, eroded	25.8	59.4	14.8	6.88	10.3%
7280	Tomek silt loam, 0 to 2 percent slopes	32.3	61.6	6.1	47.23	70.8%
7340	Filbert silt loam, 0 to 1 percent slopes	41.4	51.7	6.9	9.34	14.0%
Total Area of Field					66.69	100.0%

818

819

820

821

822

823

824

825

826

827

828

Table 2. Bounds of the van Genuchten parameters used for inverse modeling.

Soil Parameter	θ_r (-)	θ_s (-)	α (1/cm)	n (-)	K_s (cm/day)	l (-)
Range	0.03–0.30	0.3–0.6	0.001–0.200	1.01–6.00	1–200	-1–1

829

830

831

832

833

834

835

836

837

838

839

840

841

842

843

844 Table 3. Goodness-of-fit measures for simulated and observed *SWC* data at different depths during
 845 the calibration period (2008 to 2010) and validation period (2011-2012) at TPs locations. Note
 846 we assume a good fit as an RMSE between 0-0.03 cm³/cm³ and fair as between 0.03-0.06
 847 cm³/cm³.

Location	Depth (cm)	Calibration Period (2008-2010)				Validation Period (2011-2012)			
		R ²	MAE (cm ³ /cm ³)	RMSE (cm ³ /cm ³)	NSE	R ²	MAE (cm ³ /cm ³)	RMSE (cm ³ /cm ³)	NSE
TP 1	10	0.542	0.024	0.036	0.533	0.532	0.016	0.033	0.503
	25	0.742	0.014	0.022	0.739	0.716	0.029	0.040	0.486
	50	0.409	0.013	0.023	0.407	0.603	0.041	0.074	0.157
	100	0.352	0.015	0.022	0.343	0.419	0.027	0.038	0.358
TP 2	10	0.330	0.044	0.066	0.305	0.287	0.047	0.061	0.052
	25	0.623	0.010	0.020	0.604	0.718	0.038	0.055	0.135
	50	0.551	0.015	0.026	0.074	0.683	0.040	0.055	0.202
	100	0.424	0.019	0.027	-2.055	0.344	0.048	0.073	-0.473
TP 3	10	0.269	0.034	0.051	0.256	0.534	0.086	0.102	-4.265
	25	0.512	0.011	0.017	0.509	0.852	0.010	0.015	0.793
	50	0.549	0.015	0.023	-0.214	0.658	0.022	0.033	0.652
	100	0.238	0.018	0.029	-3.156	0.669	0.018	0.025	0.178
TP 4	10	0.412	0.029	0.044	0.406	0.580	0.051	0.071	-0.116
	25	0.434	0.016	0.025	0.350	0.594	0.029	0.042	0.490
	50	0.151	0.009	0.015	-13.400	0.443	0.041	0.073	0.036
	100	0.001	0.013	0.021	-12.058	0.292	0.026	0.039	0.238

848

849

850

851

852

853

854 Table 4. Goodness-of-fit measures for simulated and observed *SWC* data during the calibration
855 period (2012 to 2013) and validation period (2014) at CRNP location.

Location	Depth (cm)	Calibration Period (2012-2013)				Validation Period (2014)			
		R ²	MAE (cm ³ /cm ³)	RMSE (cm ³ /cm ³)	NSE	R ²	MAE (cm ³ /cm ³)	RMSE (cm ³ /cm ³)	NSE
CRNP	10	0.497	0.018	0.027	0.456	0.192	0.020	0.032	-0.310

856

857

858

859

860

861

862

863

864

865

866

867

868 Table 5. Optimized van Genuchten parameters in different locations at the study site. Note, 95%
 869 confidence intervals are in parentheses.

Location	Depth (cm)	θ_r (-)	θ_s (-)	α (1/cm)	n (-)	K_s (cm/day)	l (-)
TP 1	0-15	0.134 (0.130-0.137)	0.423 (0.417-0.429)	0.027 (0.026-0.027)	1.475 (1.456-1.494)	8.119 (7.965-8.273)	0.546 (0.525-0.567)
	15-35	0.136 (0.132-0.141)	0.408 (0.404-0.412)	0.007 (0.007-0.007)	1.345 (1.322-1.367)	11.540 (11.137-11.939)	0.480 (0.466-0.494)
	35-75	0.191 (0.188-0.194)	0.448 (0.443-0.453)	0.024 (0.024-0.025)	1.097 (1.088-1.105)	8.057 (7.879-8.235)	0.285 (0.278-0.292)
	75-175	0.071 (0.068-0.073)	0.430 (0.424-0.436)	0.025 (0.024-0.025)	1.069 (1.061-1.077)	9.807 (9.540-10.073)	0.364 (0.354-0.375)
TP 2	0-15	0.211 (0.195-0.227)	0.446 (0.431-0.461)	0.027 (0.018-0.035)	1.567 (1.431-1.703)	8.120 (4.660-11.580)	1.000 (0.411-1.589)
	15-35	0.197 (0.105-0.289)	0.434 (0.425-0.442)	0.006 (0.003-0.008)	1.191 (1.076-1.306)	8.655 (0.953-16.357)	0.022 (-0.194-0.238)
	35-75	0.110 (0-0.258)	0.424 (0.406-0.441)	0.015 (0.007-0.023)	1.239 (1.040-1.438)	4.605 (0-9.214)	0.723 (-1.210-2.655)
	75-175	0.109 (0-0.275)	0.408 (0.357-0.459)	0.020 (0-0.044)	1.302 (0.965-1.639)	6.780 (0-20.523)	0.000 (-0.045-0.045)
TP 3	0-15	0.281 (0.276-0.287)	0.464 (0.463-0.465)	0.035 (0.033-0.036)	1.487 (1.446-1.528)	7.096 (6.742-7.450)	0.400 (0.385-0.416)
	15-35	0.072 (0.069-0.075)	0.402 (0.398-0.407)	0.012 (0.011-0.012)	1.085 (1.076-1.095)	29.960 (28.470-31.457)	0.353 (0.340-0.367)
	35-75	0.081 (0.076-0.087)	0.498 (0.481-0.515)	0.037 (0.034-0.039)	1.128 (1.108-1.149)	24.440 (22.013-26.872)	0.527 (0.472-0.583)
	75-175	0.085 (0.077-0.092)	0.500 (0.482-0.518)	0.039 (0.036-0.042)	1.147 (1.124-1.170)	17.540 (15.995-19.088)	0.496 (0.454-0.539)
TP 4	0-15	0.082 (0.069-0.096)	0.481 (0.474-0.489)	0.034 (0.030-0.038)	1.172 (1.158-1.186)	7.773 (6.913-8.632)	0.953 (0.772-1.133)
	15-35	0.200 (0.175-0.225)	0.426 (0.420-0.433)	0.013 (0.010-0.017)	1.217 (1.173-1.262)	14.060 (9.248-18.873)	0.044 (0.027-0.061)
	35-75	0.250 (0.240-0.260)	0.477 (0.472-0.481)	0.009 (0.007-0.011)	1.079 (1.066-1.092)	1.045 (0.952-1.138)	0.353 (0.168-0.538)
	75-175	0.200 (0.185-0.214)	0.487 (0.481-0.494)	0.012 (0.009-0.014)	1.070 (1.057-1.083)	1.454 (1.146-1.762)	0.985 (0.706-1.264)
CRNP	0-15	0.100 (0.098-0.103)	0.392 (0.386-0.398)	0.019 (0.018-0.019)	1.054 (1.145-1.164)	6.931 (6.786-7.076)	0.547 (0.545-0.549)

870

871
872

Table 6. Goodness-of-fit measures for simulated and observed daily ET_a during the simulation period (2007-2012) at study site.

Location	R^2	MAE (mm/day)	RMSE (mm/day)	NSE
ET_p	0.510	1.359	1.992	0.340
TP 1	0.644	0.696	1.062	0.618
TP 2	0.754	0.610	0.907	0.746
TP 3	0.751	0.601	0.904	0.728
TP 4	0.365	0.878	1.387	0.168
TPs Weighted Average	0.742	0.599	0.911	0.714
CRNP	0.573	0.742	1.143	0.562

873

874

875

876

877

878

879

880

881

882

883

884

885

886 Table 7. Summary of simulated yearly and average actual evapotranspiration (ET_a) (mm) and
 887 observed yearly and average actual evapotranspiration (ET_a) (mm) from Eddy-Covariance
 888 tower during 2007 to 2012.

Location	Year						
	2007	2008	2009	2010	2011	2012	Average
ET_p	1048.5	987.9	989.4	1011.5	1025.7	1326.7	1064.9
EC	656.8	608.4	589.7	646.1	622.2	570.1	612.5
TP 1	646.1	629.0	559.8	642.1	573.9	415.5	579.5
TP 2	614.3	598.4	576.7	620.5	576.9	429.5	574.7
TP 3	529.0	556.1	556.4	590.4	549.8	405.2	545.4
TP 4	652.2	576.1	529.9	677.3	458.2	381.2	525.3
Upscaled TPs	613.9	564.1	556.3	600.3	547.7	405.9	548.0
CRNP	745.3	707.1	603.0	721.8	642.2	439.3	643.1

889